Petroleum Science 19 (2022) 949–962

Contents lists available at ScienceDirect

Petroleum Science

journal homepage: www.keaipublishing.com/en/journals/petroleum-science

Original Paper

Study of the gas sources of the Ordovician gas reservoir in the Central-Eastern Ordos Basin

Ji-Jun Li [a], Zi-Wei Song [a], Chun-Lin Zhang [b, *], Shuang-Fang Lu [a], Mei-Jun Dong [a], Shu-Ning Zhang [a], Jun Jiang [a]

[a] Key Laboratory of Deep Oil and Gas, China University of Petroleum (East China), Qingdao, Shandong, 266580, China
[b] PetroChina Research Institute of Petroleum Exploration and Development, Beijing, 100083, China

ARTICLE INFO

Article history:
Received 9 November 2020
Accepted 30 April 2021
Available online 23 December 2021

Edited by Jie Hao

Keywords:
Ordos Basin
Majiagou Formation
Carbon isotope kinetics
Gypsum layer
Gas source

ABSTRACT

The source of the natural gas in the Lower Paleozoic Ordovician strata in the Ordos Basin, China is a controversial issue. In the present study, the genesis and distribution characteristics of the Ordovician natural gas were qualitatively investigated based on the composition of the natural gas and the hydrocarbon isotopic composition. Then, the kinetics of the carbon isotope were analyzed to determine the proportions of the gas in the Ordovician gas reservoir contributed from the Carboniferous-Permian and Ordovician strata. The results show the following. Compared to the Upper Paleozoic natural gas, the Ordovician natural gas has a large dryness coefficient. In core areas where gypsum-salt rocks are developed, the gypsum-salt rocks completely isolate the gas sources. The weathering crust of the reservoir in the fifth member of the Majiagou Formation (Ma_5^{1+2}) originates primarily from the Upper Paleozoic coal-measure source rocks, while the Ma_5^5 and the pre-salt natural gas are mainly derived from the Ordovician source rocks. In the areas where the gypsum-salt rocks are relatively well-developed, the gypsum-salt rocks isolate the gas source to some extent, the pre-salt gas reservoir is mainly derived from the Lower Paleozoic source rocks, and this contribution gradually increases with increasing depth. In the areas where the gypsum-salt rocks are not developed, the proportion of the contribution of the Upper and Lower Paleozoic source rocks to the gas source of the Ordovician gas reservoir is mainly controlled by the volume of gas generated and the other accumulation conditions, and it does not reflect the isolation effect of the gypsum-salt rocks on the gas source. The Ordovician natural gas accumulation models in the central-eastern Ordos Basin can be divided into four types according to the differences in the gas sources.

1. Introduction

The Ordos Basin is one of important gas-producing basins in China. Since the Jingbian gas field was proven to be productive, new discoveries have been continuously made in the Lower Paleozoic Ordovician strata in the central-eastern part of the basin. A daily commercial gas flow of over 10,000 m^3 has been successively obtained from wells such as wells Jintan-1, Tao-74, and Lian-92 in the east side of the paleo-uplift part of the basin with a proven reserve of 100 billion m^3, which makes it an important exploration target in the basin (Kong et al., 2019). However, there have been three different views on the source of the natural gas for a long time. The first view holds that the Ordovician marine source rocks have a low organic matter abundance and an insufficient hydrocarbon generation and expulsion capacity. Furthermore, the Ordovician natural gas is coal gas accumulated through vertical migration for hydrocarbon supply, with the gas source originating from the Upper Paleozoic Carboniferous-Permian coal-measure strata (Xia, 2002; Yang et al., 2009; Mi et al., 2012). The second view is that the Lower Paleozoic natural gas is mainly derived from the Upper Paleozoic Carboniferous-Permian coal-measure source rocks, and the oil-type gas is from the Upper Paleozoic Carboniferous limestones (Dai et al., 2005, 2014; Hu et al., 2010). The third view holds that for the pre-salt natural gas, the vertical distance from the Upper Paleozoic coal-measure source rock is large, and there is a certain thickness of gypsum-salt rock with a good sealing and isolation performance in the middle, so it is difficult for the Upper Paleozoic coal gas to back flow into the pre-salt reservoir. The density and heterogeneity of

* Corresponding author.
E-mail address: zhangcl69@petrochina.com.cn (C.-L. Zhang).

https://doi.org/10.1016/j.petsci.2021.12.023

the dolomite reservoir make it difficult for natural gas to migrate laterally from the central area where the gypsum salt was not developed to the eastern area where the gypsum salt was developed. Furthermore, the carbonate rocks of the Lower Paleozoic Majiagou Formation contain a certain proportion of effective source rocks, the organic matter is a high-quality sapropel type with a high potential for hydrocarbon generation, so the pre-salt natural gas should be self-generated and self-accumulated oil-type gas (Kong et al., 2019; Liu et al., 2016). In fact, the source rocks and gypsum-salt layers in the Upper and Lower Paleozoic strata developed differently in different areas of the basin, and thus, the Ordovician natural gas sources may be different in different areas (Ma et al., 2011; Li et al., 2008; Zhao et al., 2015). Therefore, it is necessary to investigate the division and stratification of the Ordovician natural gas sources.

Natural gas sources are mainly investigated using the natural gas composition, carbon isotope discrimination charts, and the $\delta^{13}C_1$-R_o relationship (Stahl, 1977; Schoell, 1980, 1983; Ni et al., 2019). However, these discriminant charts and models were established for a certain statistical range, which places limitations on their applicable geological settings, and thus, they cannot reproduce the evolution of natural gas carbon isotope values over geological periods. Therefore, geochemists have established a series of fractionation models based on the Rayleigh equation (Clayton and Chris, 1991; Berner et al., 1992, 1995; Rooney et al., 1995; Lorant et al., 1998, 2000). The blind investigation of the fractionation factors using this type of model makes the isotopic fractionation unrecognizable in essence. In the mid-1990s, researchers established isotope kinetic models based on chemical kinetics to consider the causes (different kinetic parameters) and influencing factors (time and temperature) of isotopic fractionation from the perspective of chemical kinetics, which resulted in important breakthroughs (Cramer et al., 1998, 2001; Gaschnitz et al., 2001; Xiong et al., 2004; Li et al., 2020).

In the present study, the distribution characteristics of the origin of the Ordovician deep natural gas in the longitudinal and transverse directions are determined and the gas sources are qualitatively investigated by means of component and isotopic composition of natural gas, and source rock geochemical analysis. Then, based on a thermal simulation experiment and using the isotope kinetic technique as the core and considering the geological setting of the natural gas accumulation, the proportions of the contribution of the two sets of strata (Carboniferous-Permian and Ordovician) to the gas source of the Ordovician gas reservoir in the central-eastern parts of the Ordos Basin are quantitatively determined in order to provide a basis for the next step in exploration and deployment.

2. Geologic setting

The central-eastern Ordos Basin refers to the vast area to the east of the central paleo-uplift, and it belongs to the northern Shaanxi slope in terms of the tectonic zone (Fig. 1). This part of the basin has an area of approximately 16×10^4 km^2. The evaporite and carbonate interactive sedimentary strata are developed extensively in the Ordovician Majiagou Formation in this area, and they are the most important carbonate gas-bearing horizon in the basin. The Ma_1 to Ma_6 members are developed from bottom to top, with a thickness of 50 to 1000 m, constituting multiple regression-transgression sedimentary cycles in the longitudinal direction (Fig. 1) (Xie et al., 2013; Guo et al., 2012; Shi et al., 2009; Hou et al., 2003). Among them, the Ma_5 member is further divided into 10 sub-members: Ma_5^1 to Ma_5^{10}, from top to bottom. The gypsum-salt rock is distributed in the widest range in the Ma_5^6 sub-member, which is mostly in the salt depression sedimentary facies zone in Mizhi in northern Shaanxi in the central-eastern part of the basin (Yang et al., 2014). Using the Ma_5^6 sub-member as a boundary, the strata of the Majiagou Formation in the gypsum-salt development area can be divided into the post-salt and pre-salt strata. The strata uplifted in the Late Ordovician suffered hundreds of millions of years of weathering, leaching, and denudation, and the post-salt strata formed a weathering crust that was in direct contact with the Upper Paleozoic coal-measure source rocks (Yao et al., 2016).

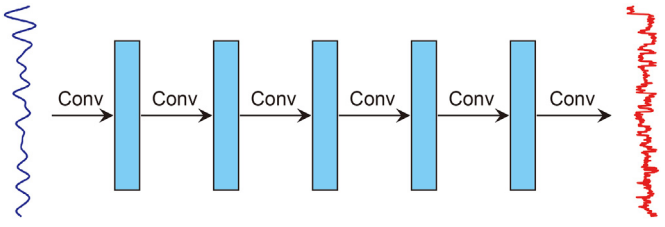

Fig. 1. Tectonic division of the Ordos Basin and comprehensive histogram of the Ordovician Majiagou Formation.

There are two sets of Paleozoic source rocks in the central-eastern Ordos Basin, namely, the Upper Paleozoic marine-terrigenous facies coal-measure source rocks and the Lower Paleozoic Ordovician marine carbonate rocks. The coal and dark mudstone are the most important Upper Paleozoic gas source rocks, and they are mainly distributed in the Lower Permian Shanxi and Taiyuan formations and the Upper Carboniferous Benxi Formation (Liu et al., 2019; Zhang, 2005). The total thickness of the coal seam is approximately 10–25 m, and the total thickness of the dark mudstone is approximately 50–150 m. The abundance of organic matter in these source rocks is relatively high. Because the Late Paleozoic was the peak period for the development of terrestrial plants, the organic matter in the Upper Paleozoic coal-measure source rocks is mainly humic (Liu et al., 2000).

The Lower Paleozoic Ordovician marine carbonate rocks in the study area are dominated by the limestone and dolomite of the Majiagou Formation. The thicknesses of the two types of source rocks are stable, ranging from 100 m to 150 m and from 150 m to 350 m, respectively. The development of the source rocks in the Majiagou Formation was controlled by stratified water bodies in a saline environment, and it is mainly found in the Ma_2 to Ma_5 members (Yu et al., 2017). The average total organic carbon content (TOC) of the source rocks in the Majiagou Formation is 0.35%, of which the organic matter abundance of the argillaceous carbonate rocks can reach 1%, and the type of kerogen is II_1 or I, which is usually in the over-mature stage (Liu et al., 2016, 2019; Chen et al., 2019). In addition, during the Middle Ordovician, the marine source rocks of the Pingliang Formation were developed on the southwestern margin of the basin. Their lithology is dominated by mudstone and marlstone. The characteristics of source rocks of Pingliang Formation are similar to those of Majiagou Formation. For both of them, the organic matter is dominated by exinite and sapropelinite, and the carbon isotope value of kerogen is −31‰ to −35‰. The source rocks is in the sedimentary environment of open platform (Zhu et al., 2011; Zhou, 2014; Dong, 2013; Li et al., 2020).

3. Samples and experiments

3.1. Samples

The samples of the Lower Paleozoic Ordovician source rocks of the Majiagou Formation are generally in the over-mature stage, and thus, they are unsuitable for thermal simulation experiments.

Therefore, the marl samples from the Pingliang Formation in the Ordos Basin, which have similar carbon isotope values, kerogen types, macerals, and sedimentary environments, were selected as substitutes in the present study. The samples were collected from an outcrop on Taitong Mountain in Pingliang, Gansu. The sample has a TOC content of 0.94%, an R_o (vitrinite reflectance) of 0.50%, and it was still in the immature stage. The identified macerals in the kerogen are mainly sapropelinite, reaching 83.1%, with a small amount of marine vitrinite and inertinite, i.e., type II_1 organic matter.

The coal and dark mudstone samples from the Shanxi, Taiyuan, and Benxi formations were selected in the present study to investigate the Upper Paleozoic Carboniferous-Permian coal-measure source rocks. Among them, the coal samples from the Shanxi Formation were from the No.5 coal seam in the Haerwusu Open-pit Coal Mine in Junggar Banner, Inner Mongolia Autonomous Region, which is geographically located on the eastern margin of the Ordos Basin. The samples have a TOC of 60.5% and an R_o of 0.54%, and thus, they are still in the immature to low mature stage. Their HI is 142 mg/g TOC. The kerogen identification shows that the macerals are dominated by vitrinite, reaching 63%, and the rest is inertinite, with a small amount of sapropelinite and exinite, i.e., type III organic matter. Gold-tube thermal simulation experiments have been previously conducted on the mudstones of the Shanxi Formation and the coals of the Taiyuan Formation (Zhang, 2005; Duan et al., 2014), and the resulting experimental data are used in the present study. The experimental data for the carbonaceous mudstone samples from the Shanxi Formation are also used to investigate the gas generation characteristics of the mudstones in the Taiyuan and Benxi formations, because of their marine-terrigenous facies sedimentary environment and similar geochemical characteristics of hydrocarbon source rocks (Wang et al., 2019). The experimental data for the coal samples from the Taiyuan Formation are also used to study the gas generation characteristics of the coals in the Benxi Formation, which have a similar sedimentary environment.

In addition, forty two natural gas samples from Ordovician in Lower Paleozoic were collected during gas testing using double valve high pressure stainless steel bottle. These samples are used for the analysis of natural gas components and stable carbon and hydrogen isotopic composition.

3.2. Experimental method

The popular gold-tube thermal simulation experiment method was used. This method advantageously uses the good plasticity of the gold tube to flexibly set and regulate the experimental pressure, and the applied pressure is exactly the internal reaction pressure of the gaps needed in the study (Landais et al., 1994; Schenk et al., 1997). The experimental equipment and sample processing method used in this study are described by Lu et al. (2019). The system was heated from 200 °C to above 600 °C at a pressure of 30 MPa, heating rates of 2 °C/h and 20 °C/h. The shut-off valve connected to the autoclave was closed at the target temperature point, the autoclave was taken out of the thermostat, and the gold tube was taken out after cooling. The gold tube was placed in a special gas collection device and punctured.

An HP 6890 gas chromatograph was used to accurately analyze the gas composition. The temperature of the injection port is 300 °C, the carrier gas is N_2, the flow rate is 1 mL/min, the split ratio is 50:1, the temperature program is set to rise from 30 °C to 260 °C, and the heating rate is 3 °C/min. An Isochrom II gas chromatography isotope ratio mass spectrometry (GC-IRMS) was used for the isotopic composition analysis. Each sample was tested at least twice, the accuracy of carbon isotopic composition analysis is ±0.3‰ (PDB standard), the accuracy of hydrogen isotopic composition analysis is ±3‰ (SMOW standard).

4. Results and discussion

4.1. Thermal simulation experiment results of the hydrocarbon generation kinetics

4.1.1. Pyrolytic gas yield characteristics

Fig. 2 shows the variation in the gas yield by pyrolysis with temperature of the Ordovician marlstone and Upper Paleozoic coal-measure source rocks in the Ordos Basin. By comparing the gas yields of the different types of source rocks, it was found that the marlstone of the Pingliang Formation has the highest methane generation capacity, followed by the coal and mudstone of the Shanxi Formation. This difference becomes more pronounced in the middle-high evolution stage. Therefore, although the Ordovician carbonate rocks in the Ordos Basin do not have a high organic matter content, they have a relatively high gas generation capacity per unit of organic matter.

4.1.2. Carbon isotope characteristics of the pyrolytic gas

Fig. 3 shows the evolution of the carbon isotope values of the methane in the pyrolytic gas from the Ordovician marlstone and Upper Paleozoic coal-measure source rocks.

As can be seen from Fig. 3, the carbon isotope values of the methane in the pyrolytic gas from the coal-measure source rocks and the marine source rocks are both affected by the pyrolysis temperature. As the temperature of the thermal simulation increased, the carbon isotope value of the methane initially decreased and then increased. At a heating rate of 20 °C/h, the lowest value of the turning point appears approximately between 410 °C and 450 °C, that is, the EasyR_o value is between 0.97% and 1.39%. At a heating rate of 2 °C/h, the lowest value of the turning point appears approximately between 380 °C and 400 °C, that is, the EasyR_o value is between 1.03% and 1.26% (Sweeney and Burnham, 1990). After the turning point, there is a good positive correlation between the $\delta^{13}C_1$ of the thermal simulation gas and the pyrolysis temperature. This is consistent with the variation in the methane carbon isotope values in thermal simulation experiments reported in other studies (Rooney et al., 1995; Cramer et al., 1998, 2001; Xiong et al., 2004; Shuai et al., 2003a). This is mainly due to the heterogeneity of the organic matter in the experimental samples (Liu et al., 2000; Sun et al., 2001). The samples used in the experiment conducted in this study contained type II and III organic matter, and their macerals both showed significant heterogeneity. Different macerals have different activation energies and times for hydrocarbon generation as well as different isotopic compositions. In addition, the special chemical structure of the parent material in kerogen is also an important reason for the complex variation of carbon isotope values of methane. In the early stage of organic matter evolution, the main way is to remove the carboxylic and heteroatom groups, and at the same time, the fatty side chain with rich ^{12}C breaks, while in the middle and high evolution stage, the aromatic ring with rich ^{13}C condenses into hydrocarbon (Shuai et al., 2003b).

4.2. Modeling and calibration of carbon isotopic fractionation kinetics

The complexity of the source, the composition, and the structure of the sedimentary organic matter (kerogen) means that it has many types of chemical bonds. The overall reaction and the series reaction models are only applicable to organic matter with relatively uniform composition and properties, while the parallel first-

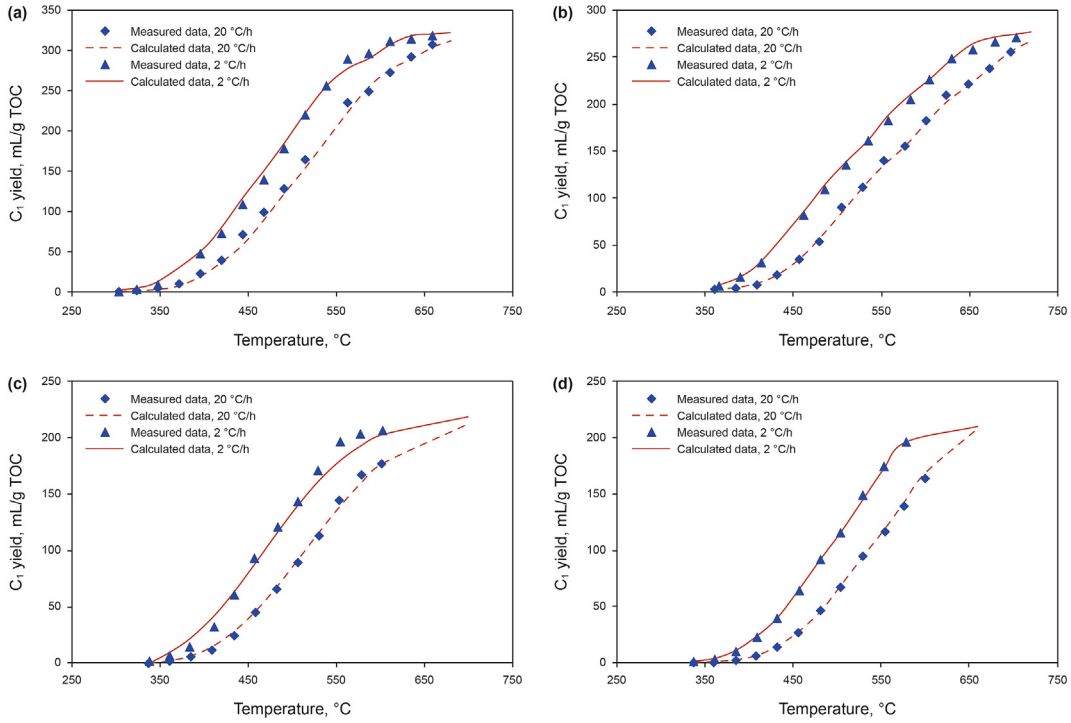

Fig. 2. Methane yield curves for the Ordos Basin samples. (**a**) Ordovician Pingliang Formation marlstone, (**b**) Shanxi Formation coal, (**c**) Shanxi Formation mudstone (measured data from Zhang, 2005), and (**d**) Taiyuan Formation coal (measured data from Duan et al., 2014).

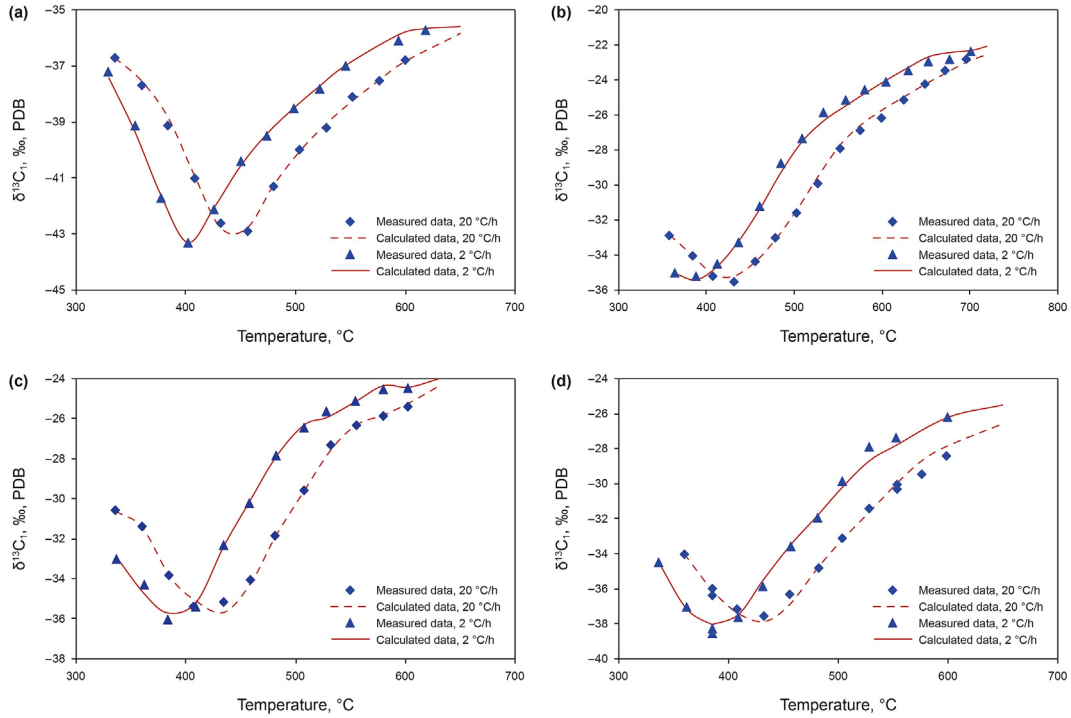

Fig. 3. Evolution curves of the methane carbon isotope values of the Ordos Basin samples. (**a**) Ordovician Pingliang Formation marlstone, (**b**) Shanxi Formation coal, (**c**) Shanxi Formation mudstone (measured data from Zhang, 2005), and (**d**) Taiyuan Formation coal (measured data from Duan et al., 2014).

order reaction model contain multiple reactions in parallel, each of which corresponds to one or a group of components with similar properties, and thus, it is more widely applicable (Li, 2008; Li et al., 2005). The Cramer model for isotopic fractionation kinetics treats methane production as the result of n parallel first-order reactions, each of which has different production rate coefficients for ^{13}C and ^{12}C gases (Eq. (1), Cramer et al., 1998, 2001).

$$R(t)=\frac{\sum_{i=1}^{n} C_{i^{13}\mathrm{C}}(t)}{\sum_{i=1}^{n} C_{i^{12}\mathrm{C}}(t)}$$
$$=\frac{\sum_{i=1}^{n}\left(f_i^{0}{}_{^{13}\mathrm{C}}-f_i^{0}{}_{^{13}\mathrm{C}}\times\exp\left(-\int_0^t k_{i^{13}\mathrm{C}}(T(t))\mathrm{d}t\right)\right)}{\sum_{i=1}^{n}\left(f_i^{0}{}_{^{12}\mathrm{C}}-f_i^{0}{}_{^{12}\mathrm{C}}\times\exp\left(-\int_0^t k_{i^{12}\mathrm{C}}(T(t))\mathrm{d}t\right)\right)}$$
$$=\frac{\sum_{i=1}^{n}\left(f_i^{0}{}_{^{13}\mathrm{C}}-f_i^{0}{}_{^{13}\mathrm{C}}\times\exp\left(-\int_0^t A_{i^{13}\mathrm{C}}\times\exp\left(-\frac{Ea_{i^{13}\mathrm{C}}}{RT}\right)(T(t))\mathrm{d}t\right)\right)}{\sum_{i=1}^{n}\left(f_i^{0}{}_{^{12}\mathrm{C}}-f_i^{0}{}_{^{12}\mathrm{C}}\times\exp\left(-\int_0^t A_{i^{12}\mathrm{C}}\times\exp\left(-\frac{Ea_{i^{12}\mathrm{C}}}{RT}\right)(T(t))\mathrm{d}t\right)\right)} \quad (1)$$

Here, $R(t)$ is the molar ratio of $^{12}CH_4$ and $^{13}CH_4$ at time t; $Ea_{i^{12}\mathrm{C}}$ and $Ea_{i^{13}\mathrm{C}}$ are the activation energies of $^{12}CH_4$ and $^{13}CH_4$, respectively; $A_{i^{12}\mathrm{C}}$ and $A_{i^{13}\mathrm{C}}$ are the pre-exponential factors of $^{12}CH_4$ and $^{13}CH_4$, respectively; R is the gas constant (8.314 J/mol·K); T is the absolute temperature (K); $k_{i^{12}\mathrm{C}}$ and $k_{i^{13}\mathrm{C}}$ are the generation rate coefficients of $^{12}CH_4$ and $^{13}CH_4$, respectively; $C_{i^{12}\mathrm{C}}(t)$ and $C_{i^{13}\mathrm{C}}(t)$ are the cumulative productions of $^{12}CH_4$ and $^{13}CH_4$, respectively, in reaction i at time t; and $f_i^{0}{}_{^{12}\mathrm{C}}$ and $f_i^{0}{}_{^{13}\mathrm{C}}$ are the hydrocarbon generation potentials of $^{12}CH_4$ and $^{13}CH_4$, respectively, each of which is equal to the product of the corresponding reaction fraction and the total hydrocarbon generation potential.

The Cramer III model with the best application effect was selected in this study as follows. First, kinetic model of parallel first-order reaction was used to fit the conversion curve of the methane generation, and the hydrocarbon generation kinetic parameters of the methane were optimized and used to approximately replace the kinetic parameters of $^{12}CH_4$ (with only a small portion being the ^{13}C component). Furthermore, the evolution curve of the carbon isotope values of the methane was directly fitted through optimization of the kinetic parameters of $^{13}CH_4$ in Eq. (1). The ratio of the hydrocarbon generation potentials of the normal methane and the heavy carbon methane was calculated by conversion of the carbon isotope value of the methane generated ultimately. The model was calibrated using the isotope kinetic softwaredeveloped by the authors (Li, 2005, 2008).

To facilitate the comparison of the calibration results, based on our past experience in the calibration of kinetic models for organic matter hydrocarbon generation, the pre-exponential factors for the generation reaction of normal methane ($^{12}CH_4$) and heavy carbon methane ($^{13}CH_4$) were uniformly set as 6×10^{13} min^{-1}. As can be seen from Figs. 2 and 3, each of them led to a good fitting result using the experimental points, thereby demonstrating the validity of the model and laying a foundation for the practical geological application in the next step.

Fig. 4 plots the calibrated chemical kinetic parameters of the isotopic fractionation in the process of the pyrolysis of each sample into methane. As can be seen from the figure, the distributions of the activation energy of the methane generated by the different samples are different, but the distribution ranges are close to each other. Except for the relatively narrow distribution of the activation energy of the methane generated by the coal samples from the Taiyuan Formation, the distributions of the activation energies by the other samples are in the range of 200–300 kJ/mol. The average activation energies of the methane generated by the different samples are different. For the same sample, the average activation energy of the heavy carbon methane generation reaction is generally slightly higher than that of normal methane, indicating that breaking the ^{13}C–^{12}C bond is more difficult than breaking the ^{12}C–^{12}C bond. The slight difference in the distribution of the activation energy of the ^{12}C and ^{13}C methane generation reactions leads to the fractionation of the carbon isotopes during methane generation.

4.3. Investigation of the gas source of the Ordovician gas reservoir in the Ordos Basin

To investigate the gas source of the Ordovician gas reservoir, first the components and isotopic composition of the natural gas were analyzed and the geochemistry of the source rocks was analyzed, to determine the longitudinal and transverse distributions of the geochemical characteristics of the Ordovician deep natural gas and to qualitatively investigate the gas source. Furthermore, the gas source was quantitatively investigated using the isotopic fractionation kinetics.

4.3.1. Analysis of the geochemical characteristics of the natural gas

As shown in Table 1 and Fig. 5, the methane content of the hydrocarbon gases from the Lower Paleozoic Majiagou Formation in the Ordos Basin is dominant, followed by the ethane content, and occasionally a very small amount of propane. Among them, the methane content is mostly between 70% and 98%, which is a larger variation range than that of the methane content of the Upper Paleozoic rocks. The drying coefficient of the natural gas ($C_1/C_{1\text{-}5}$) is mainly related to the type and maturity of the source rocks. The drying coefficient of the natural gas from the Majiagou Formation is between 94% and 99%, with an average value of 98%, which is slightly higher than that of the Upper Paleozoic natural gas, indicating that the natural gas is mainly dryness gas.

To investigate the sealing and isolation effect of the gypsum-salt layer in the Ma_5^6 member on the gas source, the study area was divided according to the thickness of the gypsum-salt layer. The gypsum-salt rock with a thickness of >50 m is regarded as the core area of the gypsum-salt rock development. The gypsum-salt rock with a thickness of 0–50 m is considered to be the relatively well-developed area of gypsum-salt rock, and the area beyond the pinch-out line of the gypsum-salt layer is the undeveloped area of the gypsum layer (Fig. 6).

Dai (1993) summarized the main types of natural gas and presented a natural gas classification chart based on the difference in the components and properties of the different types of natural gas. As can be seen from Fig. 7a, the Upper Paleozoic natural gas exhibits the characteristics of coal-type gas. The carbon isotope data of the well locations in the study area were mapped, from which it can be seen that the Ma_5^{1+2} weathering crust reservoir is clearly biased towards coalbed methane. The outliers located in region E in the figure refer to, from top to bottom, wells Shan377 and Shan265, and are characterized by oil-type gas (Fig. 7b). Both wells are located in the gypsum-salt development area (Fig. 6). The gypsum layer effectively prevents the upward migration of pre-salt oil and gas, so the two wells are more likely to be affected by the Ma_5^5 gas source. Most of the Ma_5^5 natural gas types are oil-type pyrolytic gas, and most of the points are located in region E (Fig. 7c). This is because dolomitic mudstone and argillaceous dolomite are developed in Ma_5^5 formation. Although their thickness is not large, the TOC value is very high, mostly more than 2%, and the highest value can reach 8% (Li et al., 2017; Tu et al., 2016). A considerable portion of the natural gas is produced by its source rocks during pyrolytic hydrocarbon generation and is accumulated in the Ma_5^5 member. The two points located in regions G and H in the figure represent wells Yi5 and Tao19, respectively, indicating that part of the gas in the

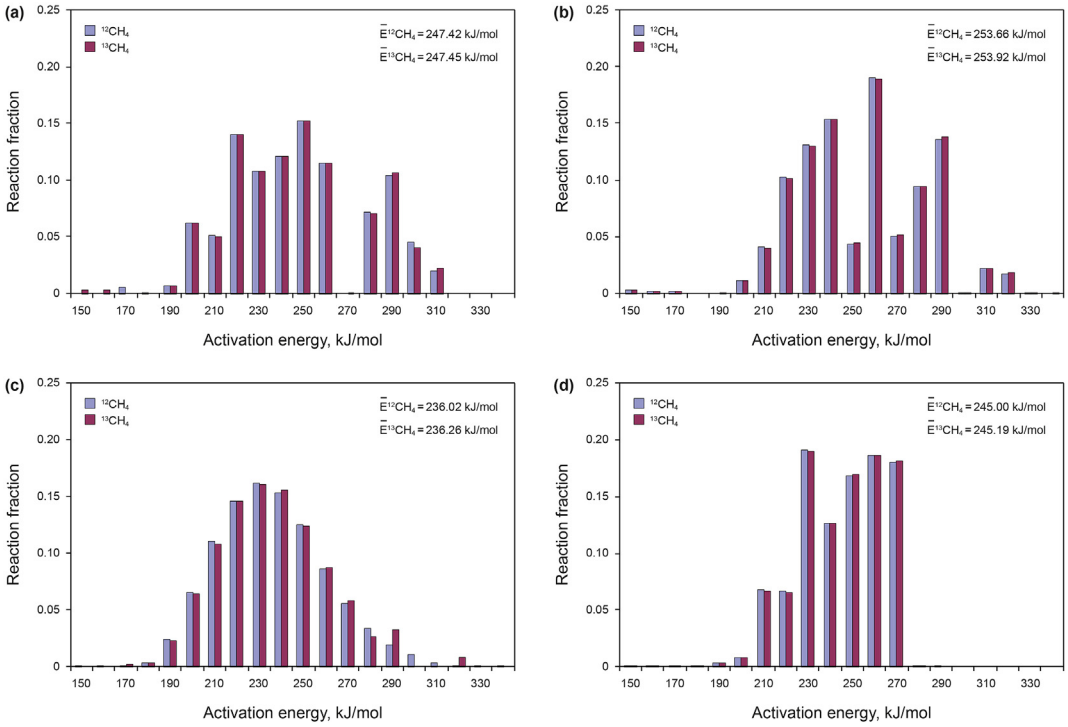

Fig. 4. Distribution of the activation energy of the methane reaction in the Ordos Basin samples. (**a**) Ordovician Pingliang Formation marlstone, (**b**) Shanxi Formation coal, (**c**) Shanxi Formation mudstone, and (**d**) Taiyuan Formation coal.

reservoir is derived from the Upper Paleozoic coal-type gas.

For Ma_5^6 and the pre-salt strata, in the core area where the gypsum salt is developed, the gas source is mainly Lower Paleozoic carbonate rock due to the isolation effect of the gypsum salt, and the generated gas is mainly oil-type pyrolytic gas. In areas where the gypsum salt is relatively well-developed or undeveloped, for the wells (e.g., wells Tong75, Chengtan3, and Shan367) in regions G and H in the figure (Fig. 7d), the Upper Paleozoic source rock contributes to the gas reservoir due to the relatively weak isolation effect of the gypsum-salt layer.

In addition, the stable hydrogen isotope values have the largest range among all the isotope values. Hydrogen isotope values are more sensitive to changes in the geochemical environment and can reflect the sedimentary environment of gas source rocks (Wang et al., 2012; He et al., 2018, 2019, 2020; Huang et al., 2019). Due to the hydrogen isotope composition of water, the δ^2H value of the continental natural gas is basically lighter than −160‰, and the δ^2H value of marine natural gas is heavier than −160‰ (Yu et al., 2013). As can be seen from Fig. 8, the hydrogen isotope values of the Ma_5^{1+2} layers of wells Jintan1 and Shuang118 are light, with values closer to the δ^2H values of the Upper Paleozoic strata, showing terrigenous characteristics. In comparison, the hydrogen isotope values of the pre-salt production horizon of wells Longtan1 and Jintan1 are heavier than −160‰, indicating that they are the products of marine source rocks, further demonstrating the sealing and isolation effect of the gypsum-salt layer.

4.3.2. Application of methane carbon isotopic fractionation kinetics

By combining the carbon isotopic kinetic parameters of the pyrolysis of the source rocks into methane with the sedimentation and burial history and the thermal history of each well, the conversion rates of $^{12}CH_4$ and $^{13}CH_4$ into oil during the geological period can be obtained. Then, the respective hydrocarbon generation potential was used to obtain the corresponding production volume and subsequently the carbon isotope value of the methane.

To explore the influence of the gypsum layer on the gas source of the Ordovician gas reservoir, a total of six wells were selected in different blocks in the central-eastern Ordos Basin for the chemical kinetics application of the natural gas generation and carbon isotopic fractionation, with 2 wells each in the core developed area, the relatively developed area, and the undeveloped areas of the gypsum layer. The gas generation history curve and the natural gas carbon isotope value evolution curve of each set of source rocks in the Upper and Lower Paleozoic strata in the study area were plotted.

The Upper and Lower Paleozoic gases were used as the two end members of the Ordovician gas source mixture. Considering the methane carbon isotope values and the gas generation intensity by each set of source rocks (Eq. (2)), the amount of normal methane and heavy carbon methane in each layer were calculated (Eqs. (3) and (4)), and accumulated, respectively.

$$Q = h \times TOC \times \rho \times I_H \times F \tag{2}$$

Here, Q is the gas generation intensity; h is the thickness of the source rock layer, which was obtained from each set of source rock contour maps (Fang, 2012; Han, 2015; Wang, 2010; Li et al., 2017, 2018; Wang et al., 2015; Liu et al., 2019). *TOC* is the original abundance of the organic matter (%), which was obtained by averaging the *TOC* after the restoration of each horizon (using the principle and method described by Lu et al., 2003). ρ is the source rock's density, which was obtained based on a common rock density table, with a coal density of 1.5 g/cm^3, a mudstone density of 2.4 g/cm^3, and a carbonate density of 2.7 g/cm^3 (Huang, 2015; Xu, 2008; Meng, 2008). I_H is the original hydrogen index (mg/g.TOC), which was obtained by averaging the hydrogen indexes after the restoration of each horizon (using the principle and method described by Lu et al., 2003, 1995). F is the gas conversion rate, which was calculated from the hydrocarbon generation kinetics.

Table 1
Gaseous composition and isotopic compositions of natural gases in the Ordovician and Upper Paleozoic reserviors in the central-eastern Ordos Basin.

Area	Well	Strata	Component, %								log[C_1/(C_2+C_3)]	C_1/C_{1-5}	$\delta^{13}C$ (‰, PDB)			δ^2H (‰, VSMOW)	Data Source
			C_1H_4	C_2H_6	C_3H_8	IC_4H_{10}	NC_4H_{10}	IC_5H_{12}	NC_5H_{12}	H_2S			C_1H_4	C_2H_6	C_3H_8		
Post-salt	Shan265	$O_1m_5^1$	95.07	0.37	0.06	0.00	0.01	0.00	0.00	0.00	2.35	1.00	−30.98	−37.32	−32.81	–	This paper
	Shan377	$O_1m_5^{1,2}$	95.86	0.27	0.03	0.00	0.00	0.00	0.00	0.00	2.51	1.00	−32.92	−36.50	−29.62	–	
	Su357	$O_1m_5^1$	91.09	2.37	0.36	0.14	0.08	0.08	0.03	0.00	1.52	0.97	−33.32	−24.53	−22.94	–	
	Su360	$O_1m_5^1$	71.52	3.23	0.53	0.05	0.07	0.02	0.02	0.00	1.28	0.95	−33.95	−23.30	−26.10	–	
	Shan327	$O_1m_5^{1,2}$	96.34	0.45	0.07	0.01	0.02	0.01	0.01	0.00	2.27	0.99	−27.78	–	–	–	
	Shan339	$O_1m_5^1$	93.51	0.72	0.13	0.02	0.02	0.01	0.01	0.00	2.04	0.99	−30.63	–	–	–	
	Jintan1	$O_1m_5^1$	51.32	0.42	0.10	0.01	0.01	0.00	0.00	0.00	1.99	0.99	−33.90	−32.20	−28.80	−174.00	
	Yi6	$O_1m_5^{1,2}$	83.26	0.75	0.08	0.01	0.01	0.00	0.00	0.00	2.00	0.99	−32.60	−36.40	−32.70	–	
	Shuang113	$O_1m_5^{1,2}$	97.34	1.04	0.11	0.04	0.03	0.03	0.01	0.00	1.93	0.99	−36.00	−27.90	−26.40	–	
	Shuang118	$O_1m_5^{1,2}$	95.28	1.55	0.18	0.03	0.03	0.02	0.01	0.00	1.74	0.98	−35.20	−35.50	−32.40	−175.00	
	Tao50	$O_1m_5^5$	82.64	0.46	0.06	0.01	0.01	0.00	0.00	0.00	2.20	0.99	−34.30	−31.40	−29.90	–	
	Shan431	$O_1m_5^5$	91.13	0.29	0.02	0.00	0.00	0.00	0.00	0.00	2.48	1.00	−35.74	−26.95	−26.14	–	
	Su203	$O_1m_5^5$	90.18	0.62	0.07	0.01	0.03	0.01	0.01	0.00	2.11	0.99	−33.51	–	–	–	
	Shan310	$O_1m_5^5$	94.71	0.19	0.01	0.00	0.00	0.00	0.00	0.00	2.67	1.00	−35.15	−24.10	−25.00	–	
	Shan323	$O_1m_5^5$	93.29	0.25	0.02	0.00	0.00	0.00	0.00	0.00	2.55	1.00	−34.41	−36.31	−31.27	–	
	Su222	$O_1m_5^5$	92.26	0.27	0.03	0.00	0.00	0.00	0.00	0.00	2.49	1.00	−32.68	−28.56	−30.43	–	
	Su279	$O_1m_5^5$	89.43	0.62	0.19	0.03	0.05	0.00	0.01	0.00	2.04	0.99	−32.91	−34.71	−28.30	–	
	Zitan1	$O_1m_5^5$	90.60	0.34	0.05	0.00	0.00	0.00	0.00	0.00	2.37	1.00	−33.20	−33.90	−30.40	–	
	Shuang107	$O_1m_5^5$	95.25	1.94	0.52	0.29	0.16	0.11	0.04	0.00	1.59	0.97	−42.00	−25.20	−23.00	–	
	Yi5	$O_1m_5^5$	77.85	2.48	0.68	0.28	0.25	0.14	0.09	0.00	1.39	0.95	−35.20	−31.50	−27.30	–	
	Tao19	$O_1m_5^5$	72.82	3.29	0.69	0.13	0.12	0.05	0.02	0.00	1.26	0.94	−32.00	−22.90	−24.60	–	
	Shuang107	$O_1m_5^5$	95.25	1.94	0.52	0.29	0.16	0.11	0.04	0.00	1.59	0.97	−41.30	−25.20	−23.00	–	
	Lian45	$O_1m_5^5$	90.92	0.08	0.01	0.00	0.00	0.00	0.00	0.42	3.00	1.00	−35.00	–	–	–	
	Su292	$O_1m_5^5$	82.41	0.29	0.03	0.00	0.00	0.00	0.00	0.00	2.41	1.00	−33.00	–	–	–	
Pre-salt	Tao52	$O_1m_5^6$	83.46	0.15	0.01	0.00	0.00	0.00	0.00	0.00	2.72	1.00	−35.00	−30.30	–	–	
	Shan373	$O_1m_5^{5,6}$	92.45	0.24	0.02	0.00	0.00	0.00	0.00	0.00	2.55	1.00	−34.35	−33.65	−26.84	–	
	Shan431	$O_1m_5^6$	86.49	0.24	0.04	0.02	0.03	0.01	0.01	0.00	2.49	1.00	−35.74	−26.95	−26.14	–	
	Su381	$O_1m_5^6$	92.43	0.14	0.01	0.00	0.00	0.00	0.00	0.00	2.78	1.00	−35.95	−34.51	–	–	
	Su234	$O_1m_5^{6,7}$	31.53	0.06	0.00	0.00	0.00	0.00	0.00	0.00	2.67	1.00	−37.34	−34.03	–	–	
	Longtan1	$O_1m_5^7$	92.40	2.80	0.47	0.19	0.10	0.05	0.02	0.00	1.45	0.96	−39.40	−23.40	−19.00	−153.00	
	Longtan1	$O_1m_5^7$	92.46	2.79	0.45	0.18	0.10	0.05	0.02	0.00	1.46	0.96	−39.30	−23.40	−19.70	–	
	He3	$O_1m_5^7$	56.73	0.15	0.00	0.00	0.00	0.00	0.00	0.00	2.58	1.00	−35.70	−35.50	–	–	
	Tong75	$O_1m_5^7$	92.24	1.96	0.35	0.08	0.07	0.04	0.02	0.00	1.60	0.97	−35.90	−23.80	−23.30	–	
	Tong74	$O_1m_5^7$	96.80	0.83	0.11	0.05	0.02	0.01	0.00	0.00	2.01	0.99	−39.90	−39.90	−21.70	–	
	Lian12	$O_1m_5^7$	90.76	0.07	0.01	0.00	0.01	0.00	0.01	0.28	3.05	1.00	−35.00	–	–	–	
	Lian54	$O_1m_5^7$	75.61	0.14	0.01	0.00	0.00	0.00	0.00	0.00	2.70	1.00	−35.40	−36.80	–	–	
	Tao39	$O_1m_5^8$	40.17	0.01	0.00	0.00	0.00	0.00	0.00	0.36	3.60	1.00	−35.70	–	–	–	
	Jintan1	$O_1m_5^{7,9}$	68.61	0.00	0.00	0.00	0.00	0.00	0.00	22.45	–	1.00	−36.00	−23.10	–	−146.00	
	Shan367	$O_1m_5^{8,9}$	29.81	0.10	0.02	0.00	0.00	0.00	0.00	0.00	2.38	1.00	−35.50	–	–	–	
	Tong52	$O_1m_5^{10}$	48.47	1.40	0.55	0.31	0.19	0.14	0.05	0.00	1.40	0.95	−42.60	−26.50	−25.70	–	
	Tong51	O_1m_4	70.45	1.86	0.47	0.22	0.10	0.07	0.02	0.28	1.48	0.96	−41.00	–	–	–	
	Chengtan3	$O_1m_{2,3}$	68.63	2.20	0.25	0.03	0.03	0.02	0.00	0.00	1.45	0.96	−31.10	−36.90	−37.60	–	
Upper Paleozoic	Yu24-5	P_1x	92.77	4.21	0.63	0.09	0.09	–	–	–	1.28	0.95	−32.20	−23.50	−24.90	–	Hu et al. (2007)
	Su6	P_1x	88.81	5.83	1.26	0.20	0.22	–	–	–	1.10	0.92	−33.54	−24.02	−24.72	–	Li et al. (2018)
	Su14	P_1x	96.37	1.66	0.40	0.13	0.09	–	–	–	1.67	0.98	−32.54	−23.17	−23.77	−193.00	
	Su33-18	P_1x	91.69	4.26	0.91	0.25	0.29	–	–	–	1.25	0.94	−32.31	−25.23	−23.79	−190.00	
	Su36-13	P_1x	89.49	5.41	1.16	0.22	0.25	–	–	–	1.13	0.93	−33.40	−24.70	−24.40	−193.00	
	Tao5	P_1x	91.75	5.11	0.92	0.12	0.14	–	–	–	1.18	0.94	−33.05	−23.57	−23.72	–	
	Tao6	P_1x	93.40	2.76	0.36	0.04	0.46	–	–	–	1.48	0.96	−29.00	−25.00	−27.00	–	
	Shan215	P_1x	93.60	3.79	0.55	0.08	0.08	–	–	–	1.33	0.95	−32.90	−26.00	−24.00	−193.00	
	Shan241	P_1x	92.70	3.99	0.68	0.11	0.11	–	–	–	1.30	0.95	−32.60	−24.10	−24.20	–	
	Shan243	P_1x	90.85	5.46	1.03	0.18	0.17	–	–	–	1.15	0.93	−35.00	−24.00	−23.60	–	
	Wu22-7	P_1x	92.97	4.27	0.76	0.11	0.11	–	–	–	1.27	0.95	−32.60	−23.70	−24.20	–	
	Yu19-5	P_1x	92.79	3.90	0.64	0.10	0.09	–	–	–	1.31	0.95	−34.50	−23.70	−24.70	–	
	Su1	P_1s	91.57	4.52	0.89	0.19	0.16	–	–	–	1.23	0.94	−34.37	−22.13	−21.77	–	
	Shan141	P_1s	94.12	3.40	0.50	0.06	0.07	–	–	–	1.38	0.96	−33.70	−26.30	−24.30	–	
	Shan143	P_1s	93.47	3.90	0.63	0.09	0.10	–	–	–	1.31	0.95	−33.57	−25.98	−24.42	–	
	Yu28-12	P_1s	94.25	3.25	0.47	0.06	0.07	–	–	–	1.40	0.96	−32.40	−27.00	−24.80	–	
	Yu35-8	P_1s	95.32	2.67	0.34	0.07	0.06	–	–	–	1.50	0.97	−32.55	−24.87	−23.69	–	
	Yu43-10	P_1s	94.39	2.73	0.41	0.08	–	–	–	–	1.48	0.97	−31.90	−26.40	−23.00	−185.00	
	Yu44-7	P_1s	95.65	2.65	0.32	0.04	0.04	–	–	–	1.51	0.97	−32.80	−25.50	−23.80	−185.00	
	Yu69	P_1s	94.93	2.85	0.40	0.06	0.06	–	–	–	1.47	0.97	−32.80	−26.30	−24.10	−179.00	
	Zhou28-43	P_1s	90.44	5.42	1.54	0.31	0.34	–	–	–	1.11	0.93	−33.00	−23.20	−22.40	−175.00	
	Shi12	C_2b	95.31	0.53	0.04	–	–	–	–	–	2.22	0.98	−30.60	−37.20	−35.80	−165.00	
	Shi37	C_2b	96.60	0.42	0.03	–	–	–	–	–	2.33	0.98	−30.80	−37.10	−37.30	−170.00	

$$\frac{Q_i^{13}}{Q_i^{12}} = \left(\delta^{13}C_i \Big/ 1000 + 1\right) \times R_{St} \tag{3}$$

$$Q_i^{13} + Q_i^{12} = Q_i \tag{4}$$

Here, Q_i^{13} is the ^{13}C gas generation intensity of the source rock of layer i; Q_i^{12} is the ^{12}C gas generation intensity of the source rock of layer i; Q_i is the gas generation intensity of the source rock of layer i; $\delta^{13}C_i$ is the final cumulative isotope value of methane generated from source rocks of layer i determined by the combination of carbon isotopic kinetic parameters and geothermal history of each well; R_{St} is 1123.72×10^{-5}.

Subsequently, the overall isotope value of the gas produced by the Upper and Lower Paleozoic source rocks was obtained according the definition of isotope values with Eq. (5).

$$\delta^{13}C(‰, PDB) = \left(\frac{R_{Sa}}{R_{St}} - 1\right) \times 1000 = \left(\frac{\sum Q_i^{13}}{\sum Q_i^{12} \times R_{St}} - 1\right) \times 1000 \tag{5}$$

Finally, the calculation values were combined with the measured values of the natural gas from the gas reservoir to obtain the proportions of the contribution of the Upper and Lower Paleozoic source rocks to the natural gas source of each well area using Eq. (6).

$$\delta^{13}C_{mv} = \delta^{13}C_{up} \cdot x + \delta^{13}C_{lp} \cdot (1 - x) \tag{6}$$

Here, $\delta^{13}C_{mv}$ is the measured value of natural gas in each well; $\delta^{13}C_{up}$ is the total isotope value of the upper Paleozoic gas; $\delta^{13}C_{lp}$ is the overall isotope value of the lower Paleozoic gas; x is the contribution ratio of the upper Paleozoic source rock to the natural gas source.

4.3.2.1. Core area of the gypsum-salt rock development. Fig. 9a and b shows the carbon isotope value curves of the natural gas from well Longtan1. The $\delta^{13}C_1$ of the natural gas produced by the Upper Paleozoic coal-measure source rocks ranges from −36.79‰ to −32.86‰, and the $\delta^{13}C_1$ of the natural gas produced by the Ordovician Majiagou Formation marlstone ranges from −40.97‰ to −38.73‰. Comprehensive calculations were carried out by combining with the gas generation intensity by each set of source rocks. The overall $\delta^{13}C_1$ of the natural gas produced by the Upper Paleozoic coal-measure source rocks was −35.76‰, and the overall $\delta^{13}C_1$ of the natural gas produced by the Ordovician Majiagou Formation source rocks was −39.34‰. The measured $\delta^{13}C_1$ value of the natural gas from well Longtan1 in the $Ma5^7$ gas reservoir is known to be approximately −39.40‰, which is consistent with the isotope value of the natural gas produced in the Majiagou Formation source rocks, indicating that the gas reservoir in this well area is entirely derived from the Lower Paleozoic Ordovician source rock.

Likewise, the $\delta^{13}C_1$ of the natural gas generated by the Upper Paleozoic coal-measure source rocks in well Shuang118 ranges from −36.18‰ to −32.74‰. Based on a comprehensive calculation by combining with the gas generation intensity by each set of source rocks, the overall $\delta^{13}C_1$ of the natural gas generated by the Upper Paleozoic coal-measure source rocks is −35.42‰. The $\delta^{13}C_1$ of the natural gas generated by the Ordovician Majiagou Formation Ma_5^5 source rock is −41.12‰ (Fig. 9c and d). The measured value of the $\delta^{13}C_1$ of the natural gas of the Ma_5^{1+2} gas reservoir in well Shuang118 is known to be approximately −35.20‰, which is similar to the isotopic value of the natural gas produced by the Upper Paleozoic source rock, indicating that the gas reservoir in this well area entirely originates from the Upper Paleozoic source rock. In summary, in the core area of the gypsum-salt rock development, the gypsum-salt layer completely isolates the gas source.

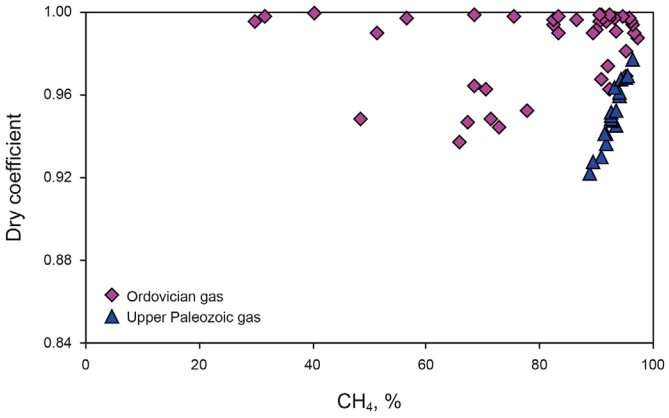

Fig. 5. Plot of CH_4 content vs dryness coefficient ($C_1/C_{1\text{-}5}$) of natural gas in the Ordovician and Upper Paleozoic.

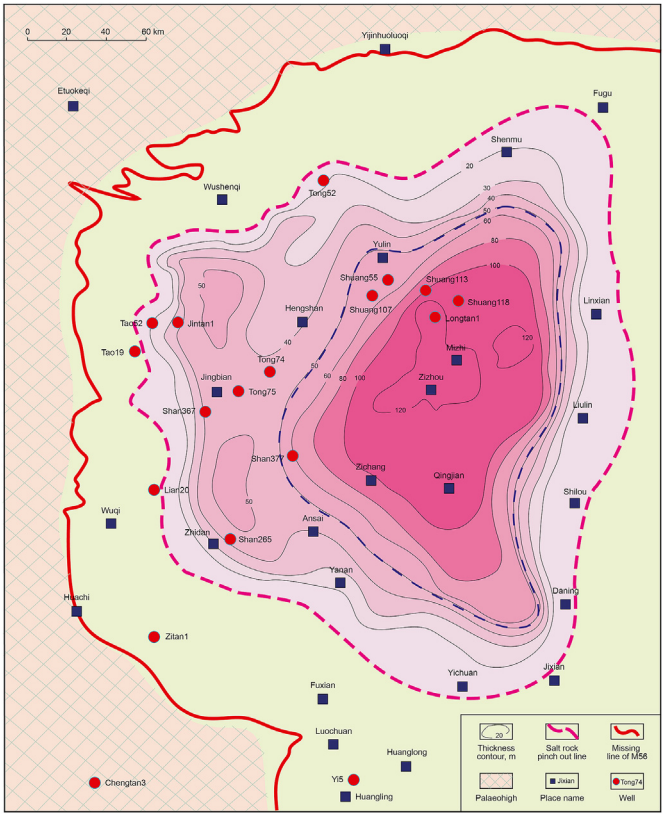

Fig. 6. Thickness of salt in the Ma_5^6 sub-member of the Majiagou Formation in the Ordos Basin.

4.3.2.2. Relatively developed area of gypsum-salt rock. The $\delta^{13}C_1$ of the natural gas generated by the Upper Paleozoic coal-measure source rocks in well Jintan1 ranges from −34.34‰ to −29.30‰, and the $\delta^{13}C_1$ of the natural gas derived from the marlstone of the Ordovician Majiagou Formation ranges from −39.17‰ to −37.73‰. Based on a comprehensive calculation considering the gas

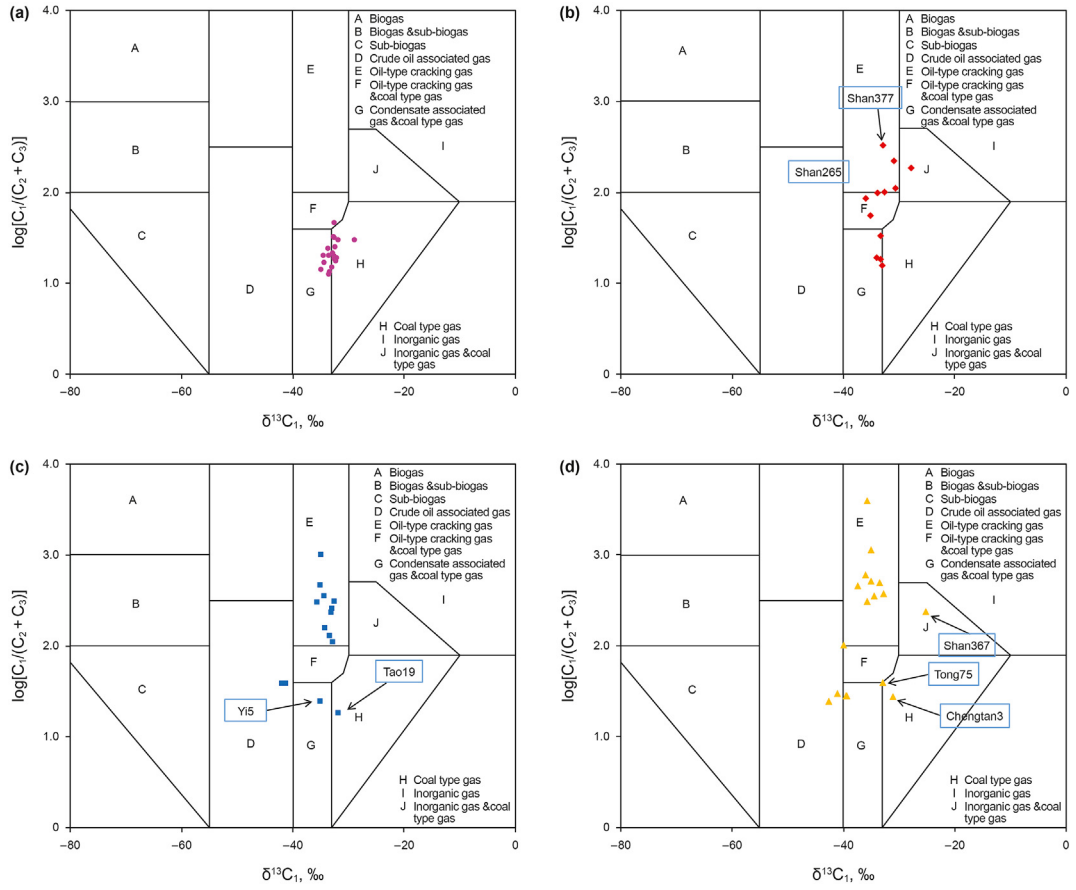

Fig. 7. Identification of the natural gas types in the Upper Paleozoic and Ordovician production horizons in the central-eastern Ordos Basin. (**a**) Upper Paleozoic, (**b**) Ma_5^{1+2} production horizon, (**c**) Ma_5^5 production horizon, and (**d**) Ma_5^6 and pre-salt production horizons.

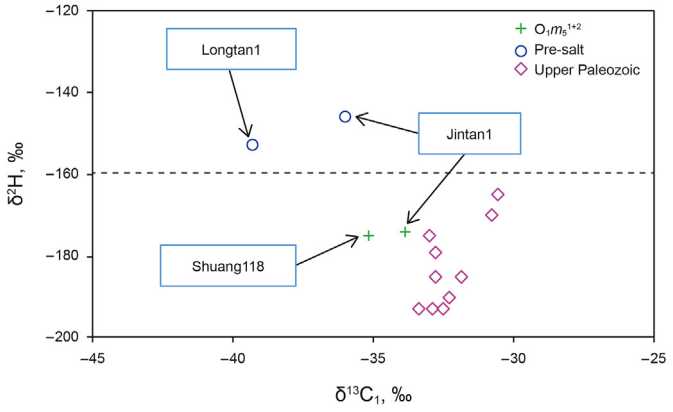

Fig. 8. Relationship between $\delta^{13}C_1$ and δ^2H for gases from the Upper Paleozoic and Lower Paleozoic post-salt and pre-salt strata in Ordos Basin, China (data from Table 1).

generation intensity by each set of source rocks, the overall $\delta^{13}C_1$ of the natural gas produced by the Upper Paleozoic coal-measure source rocks is −32.40‰, and the overall $\delta^{13}C_1$ of the natural gas produced by the Ordovician Majiagou Formation source rocks is −38.22‰ (Fig. 10a, Fig. 10b). It is known that the measured $\delta^{13}C_1$ value of the natural gas in well Jintan1 in the Ma_5^1 gas reservoir is approximately −33.90‰, and the calculated proportion of the contribution of the Majiagou Formation to the gas reservoir in the well area is approximately 22%, which is smaller than that of the Upper Paleozoic source rocks. Furthermore, the measured $\delta^{13}C_1$ value of the natural gas in well Jintan1 in the Ma_5^7 and Ma_5^9 gas reservoirs is approximately −36‰, and the calculated proportion of the contribution of the Majiagou Formation to the gas reservoir in this well area is approximately 62%, which is greater than that of the Upper Paleozoic source rocks. Considering that TSR reaction makes carbon isotope value heavier, Majiagou Formation should contribute more to the gas reservoir because of the high content of H_2S in the Ma_5^7 and Ma_5^9 of this well area.

The $\delta^{13}C_1$ of the natural gas generated by the Upper Paleozoic coal-measure source rocks in well Tao52 ranges from −33.78‰ to −28.77‰, and the $\delta^{13}C_1$ of the natural gas derived from the Ordovician Majiagou Formation source rocks ranges from −38.96‰ to −38.47‰. Based on a comprehensive calculation with the gas generation intensity from each set of source rocks, the overall $\delta^{13}C_1$ of the natural gas produced by the Upper Paleozoic coal-measure source rocks is −31.70‰, and the overall $\delta^{13}C_1$ of the natural gas produced by the Ordovician Majiagou Formation source rocks is −38.63‰ (Fig. 10c and d)). The measured $\delta^{13}C_1$ value of the natural gas in well Tao52 in the Ma_5^6 gas reservoir is known to be approximately −35‰, and the calculated proportion of the contribution of the Majiagou Formation to the gas reservoir in this well area is approximately 48%, which is close to the contribution of the Upper Paleozoic source rocks. In summary, in the area where gypsum-salt rocks are relatively developed, the gypsum-salt layer has a certain isolation effect on the gas source. From Ma_5^1 to Ma_5^7 and Ma_5^9, the contribution of the Upper Paleozoic source rocks gradually decreases, while the contribution of the Lower Paleozoic source rocks gradually increases.

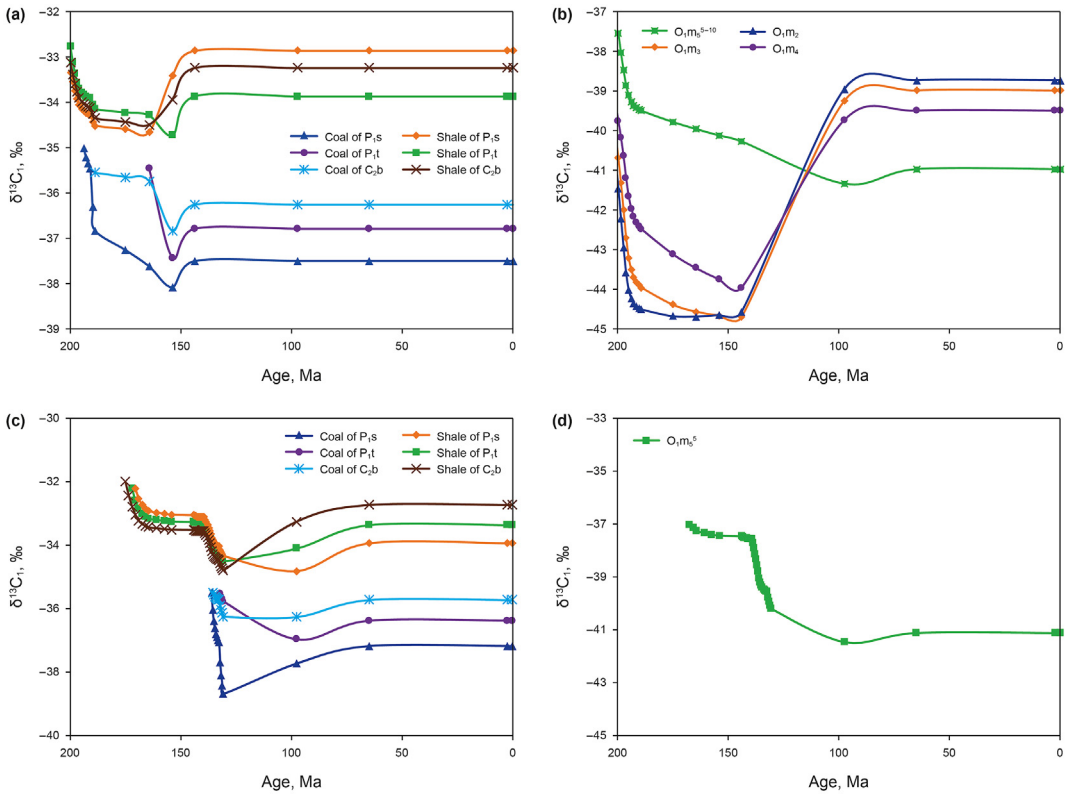

Fig. 9. Modeled carbon isotope values of methane cumulatively generated by various source rocks. (**a**) Upper Paleozoic in well Longtan1, (**b**) Majiagou Formation in well Longtan1, (**c**) Upper Paleozoic in well Shuang118, and (**d**) Majiagou Formation in well Shuang118.

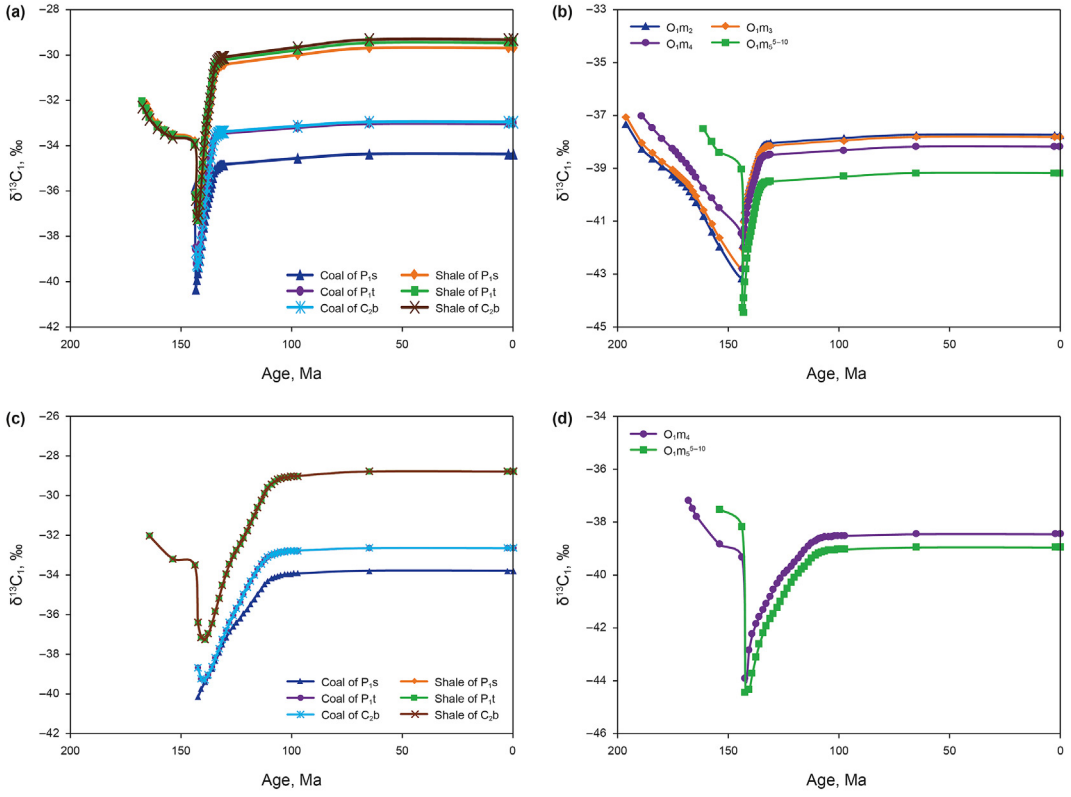

Fig. 10. Modeled carbon isotope values of methane cumulatively generated by various source rocks. (**a**) Upper Paleozoic in well Jintan1, (**b**) Majiagou Formation in well Jintan1, (**c**) Upper Paleozoic in well Tao52, and (**d**) Majiagou Formation in well Tao52.

4.3.2.3. Undeveloped area of gypsum-salt rock. The $\delta^{13}C_1$ of the natural gas generated by the Upper Paleozoic coal-measure source rocks in well Chengtan3 ranges from −32.42‰ to −26.78‰, and the $\delta^{13}C_1$ of the natural gas produced by the Ordovician Majiagou Formation marlstone ranges from −38.86‰ to −38.76‰. Based on a comprehensive calculation with the gas generation intensity by each set of source rocks, the overall $\delta^{13}C_1$ of the natural gas produced by the Upper Paleozoic coal-measure source rocks is −29.39‰, and the overall $\delta^{13}C_1$ of the natural gas produced by the Ordovician Majiagou Formation source rocks is −38.80‰ (Fig. 11a, Fig. 11b). The measured $\delta^{13}C_1$ value of the natural gas in well Chengtan3 in the Ma_2 and Ma_3 gas reservoirs is known to be approximately −31.10‰, and the calculated proportion of the contribution of the Majiagou Formation to the gas reservoir in this well area is only 18%, which is far less than that of the Upper Paleozoic source rocks. This is mainly because the Lower Paleozoic source rocks develop poorly and the amount of gas generated from the Upper Paleozoic source rocks is much higher than that generated by the Lower Paleozoic source rocks (Wang et al., 2015; Li et al., 2018; Du et al., 2019; Liu et al., 2019).

The $\delta^{13}C_1$ of the natural gas produced by the Upper Paleozoic coal-measure source rocks in well Lian20 ranges from −30.71‰ to −26.36‰. Based on a comprehensive calculation with the gas generation intensity by each set of source rocks, the overall $\delta^{13}C_1$ of the natural gas produced by the Upper Paleozoic coal-measure source rocks is −28.26‰, and the $\delta^{13}C_1$ of the natural gas generated by the Ordovician Majiagou Formation Ma_5^5 source rocks is −37.70‰ (Fig. 11c and d). The measured $\delta^{13}C_1$ value of the natural gas in well Lian20 in the Ma_5^7 gas reservoir is known to be approximately −33.60‰, and the calculated proportion of the contribution of the Majiagou Formation to the gas reservoir in this well area is approximately 57%, which is slightly higher than that of the Upper Paleozoic source rocks. This is related to the relatively well-developed Lower Paleozoic source rocks in the area around well Lian20 (Wang et al., 2015). In summary, in the area where the gypsum-salt rocks are not developed, since there is no isolation effect from the gypsum-salt rocks, the gas source mainly depends on the gas generation capacities of the Upper and Lower Paleozoic source rocks.

4.4. Hydrocarbon accumulation models

Based on the above results, the Ordovician natural gas accumulation models for the central-eastern Ordos Basin can be categorized into four types (Fig. 12). The first type of model states that in the main hydrocarbon production period (Early Jurassic to Late Cretaceous) of the Carboniferous-Permian coal-measure source rocks, under the remaining pressure difference between the source rocks and the reservoir, the natural gas migrates vertically downward along the paleo-trenches and unconformities and accumulates in the weathering crust reservoir to form a large stratigraphic-lithologic gas reservoir (Yang et al., 2011; Yang and Huang, 2019). The gas reservoir is widely distributed, and the gas-bearing horizon is stable with good continuity. The second type of model states that in the undeveloped gypsum-salt rock area in the middle, the Upper Paleozoic coal-measure strata are in direct contact with the strata below the Ma_5^6, and the natural gas produced migrates vertically into the Lower Ordovician reservoir and then laterally over a short distance. The third type of model states that in the area where the gypsum-salt rocks are relatively developed, part of the Upper

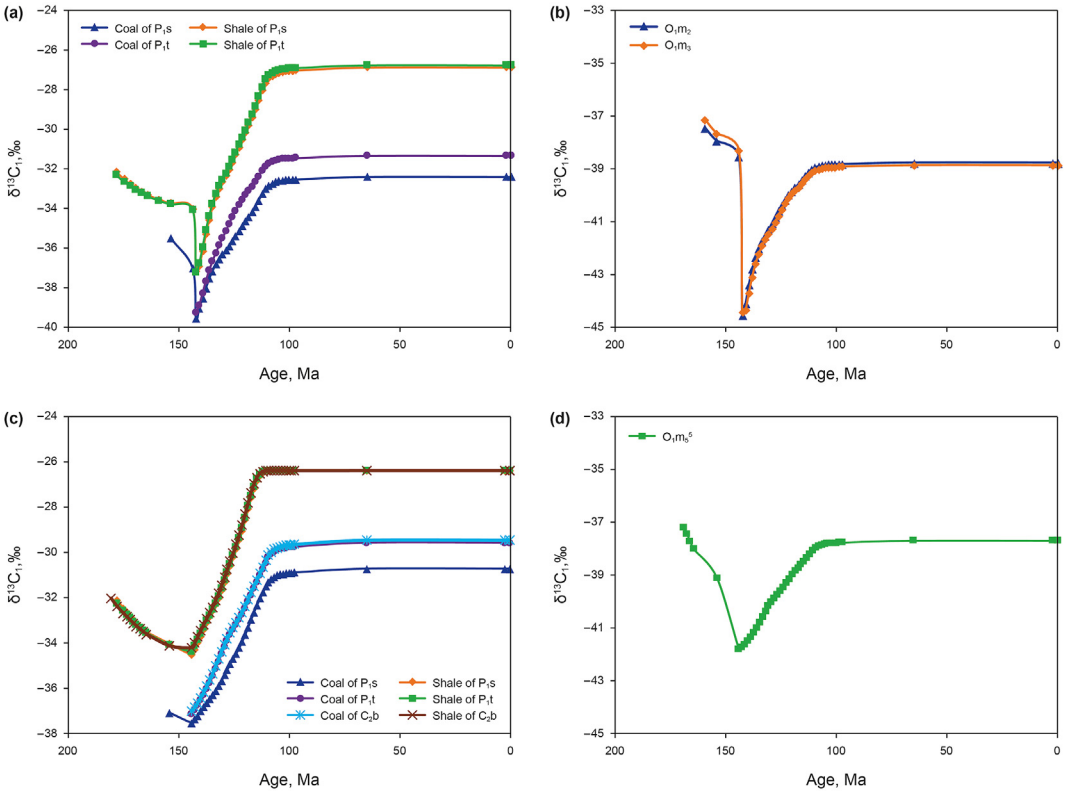

Fig. 11. Modeled carbon isotope values of methane cumulatively generated by various source rocks. (**a**) Upper Paleozoic in well Chengtan3, (**b**) Majiagou Formation in well Chengtan3, (**c**) Upper Paleozoic in well Lian20, and (**d**) Majiagou Formation in well Lian20.

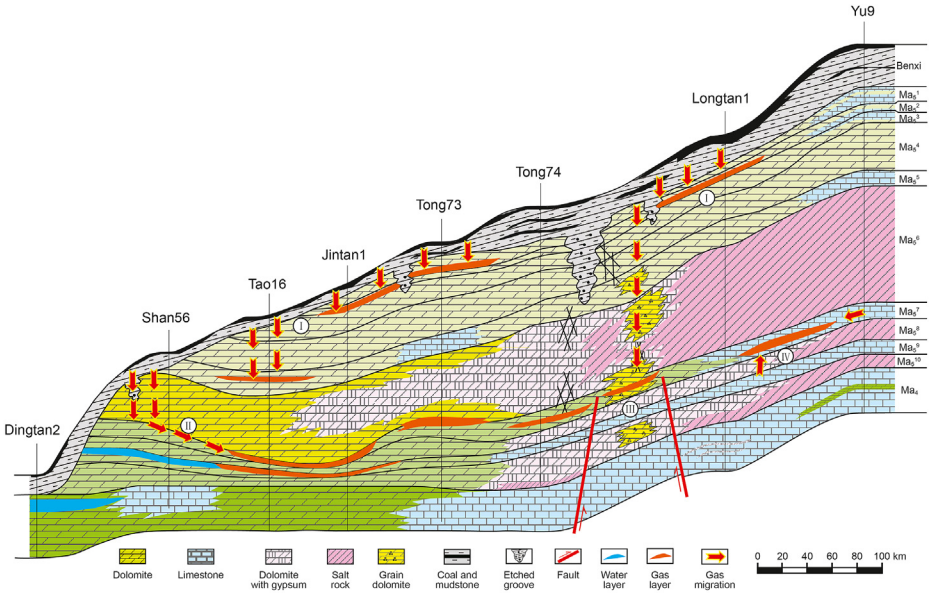

Fig. 12. Connecting-well section of source–reservoir relationship between pre-salt reservoirs and Upper Paleozoic coal measures (modified from Yang et al., 2014 and Fu et al., 2019).

Paleozoic natural gas passes vertically through the gypsum-salt cyclothem and accumulates in the Ordovician pre-salt reservoir. The second and third types of accumulation models mostly result in the mixed accumulation of natural gas generated from the Upper and Lower Paleozoic source rocks. The two types of gas reservoirs are discontinuous in distribution and are characterized by local high production and enrichment. The fourth type of model states that in the core area where the gypsum-salt rocks are developed, the pre-salt strata forms self-generated and self-stored oil-type gas reservoirs.

5. Conclusions

(1) According to the carbon and hydrogen isotopic composition characteristics, the Ma_5^{1+2} weathering crust production horizon contains continental sedimentary coal-type gas, while the Ma_5^5 and pre-salt production horizons are dominated by marine sedimentary oil-type gas.

(2) In the core area where gypsum-salt rocks are developed, the gypsum-salt rocks have a complete isolation effect on the gas source. The natural gas in the post-salt Ma_5^{1+2} weathering crust reservoir is mainly derived from the Upper Paleozoic source rocks, while the natural gas in the Ma_5^5 and pre-salt strata mainly originates from the Ordovician source rocks.

(3) In the areas where gypsum-salt rocks are relatively developed, the gypsum-salt rocks have a certain isolation effect on the gas source. From Ma_5^1 to Ma_5^6 and to Ma_7^7 and Ma_7^9, the contribution of the Upper Paleozoic source rocks gradually decreases, and the contribution of the Lower Paleozoic source rocks gradually increases.

(4) In the areas where gypsum-salt rocks are not developed, the proportions of the contributions of the Upper and Lower Paleozoic source rocks to the gas source of the Ordovician gas reservoir are mainly controlled by the degree of development of the source rocks, which does not reflect the isolation effect of the gypsum-salt on the gas source.

(5) Investigation involving the integration of the natural gas isotopic fractionation kinetics with geological and geochemical characteristics provides an effective way of studying natural gas sources.

Acknowledgements

We thank the National Natural Science Foundation of China (42172145), Prospective and Basic Research Project of CNPC (2021DJ0503), Strategic Priority Research Program of the Chinese Academy of Sciences (XDA14010403), and China National Science and Technology Major Project (2016ZX05007-002) for financial support of this study.

References

Bener, U., Faber, E., Stahl, W., 1992. Mathematical simulation of the carbon isotopic fractionation between huminitic coals and related methane. Chem. Geol. 94 (4), 315–319. https://doi.org/10.1016/0168-9622(92)90006-V.

Bener, U., Faber, E., Scheeder, G., et al., 1995. Primary cracking of algal and landplant kerogens:Kinetic models of isotope variations in methane, ethane and propane. Chem. Geol. 126 (3–4), 233–245. https://doi.org/10.1016/0009-2541(95)00120-4.

Clayton, Chris, 1991. Carbon isotope fractionation during natural gas generation from kerogen. Mar. Petrol. Geol. 8 (2), 232–240. https://doi.org/10.1016/0264-8172(91)90010-X.

Cramer, B., Krooss, B.M., Littke, R., 1998. Modelling isotope fractionation during primary cracking of natural gas: a reaction kinetic approach. Chem. Geol. 149 (3–4), 235–250. https://doi.org/10.1016/S0009-2541(98)00042-4.

Cramer, B., Faber, E., Gerling, P., et al., 2001. Reaction kinetics of stable carbon isotopes in natural gas–Insights from dry open system pyrolysis experiments. Energy Fuels 15 (3), 130. https://doi.org/10.1021/ef000086h.

Chen, J.P., Wang, X.L., Ni, Y.Y., et al., 2019. Genetic type and source of natural gas in the southern margin of Junggar Basin, NW China. Petrol. Explor. Dev. 46 (3), 482–495. https://doi.org/10.1016/S1876-3804(19)60029-7.

Dai, J.X., 1993. Hydrocarbon isotope characteristics of natural gas and identification of various types of natural gas. Nat. Gas Geosci. 4 (2), 1–40 (in Chinese).

Dai, J.X., Li, J., Luo, X., et al., 2005. Stable carbon isotope compositions and source rock geochemistry of the giant gas accumulations in the Ordos Basin,China. Org. Geochem. 36 (12), 1617–1635. https://doi.org/10.1016/j.orggeochem.2005.08.017.

Dai, J.X., Ni, Y.Y., Hu, G.Y., et al., 2014. Stable carbon and hydrogen isotopes of gases from the large tight gas fields in China. Science in China D: Earth Sci. D57, 88–103. https://doi.org/10.1007/s11430-013-4701-7.

Dong, H., 2013. Distribution and Evaluation of Hydrocarbon Source Rocks in the Southwest Margin of Erdos Basin. Chang'an University. https://doi.org/10.7666/d.D407197 (in Chinese).

Du, J.H., Li, X.B., Bao, H.P., et al., 2019. Geological conditions of natural gas accumulation and new exploration areas in the Mesoproterozoic to Lower Paleozoic

of Ordos Basin, NW China. Petrol. Explor. Dev. 46 (5), 866–882. https://doi.org/10.1016/S1876-3804(19)60246-6.
Duan, Y., Zhao, Y., Cao, X.X., et al., 2014. Carbon isotopic evolution and dynamic characteristics of pyrolysis methane. J. China Univ. Min. Technol. 43 (1), 64–71 (in Chinese).
Fang, C.Q., 2012. Evaluatian of the Reservoir-Forming Conditions of Shale Gas Potential of the UPPer Paleozoie in Eastern Ordos Basin. Xi'an Shiyou University. https://doi.org/10.7666/d.d217610 (in Chinese).
Fu, J.H., Fan, L.Y., Liu, X.S., et al., 2019. New progresses, prospects and countermeasures of natural gas exploration in the Ordos Basin. Chin. Petrol. Explor. 24 (4), 418–430. https://doi.org/10.3969/j.issn.1672-7703.2019.04.002 (in Chinese).
Gaschnitz, R., Krooss, B.M., Gerling, P., et al., 2001. On-line pyrolysis-GC-IRMS: isotope fractionation of thermally generated gases from coals. Fuel 80 (15), 2139–2153. https://doi.org/10.1016/S0016-2361(01)00095-3.
Guo, Y.R., Zhao, Z.Y., Fu, J.H., et al., 2012. Sequence lithofacies paleogeography of the Ordovician in Ordos Basin, China. Acta Pet. Sin. 33 (z2), 95–109 (in Chinese).
Han, X.Q., 2015. Evaluation for upper paleozoic hydrocarbon source rock of Shanxi formation in southeastern Ordos Basin, 215 Petrochem. Ind. Technol. 22 (9), 200–201. https://doi.org/10.3969/j.issn.1006-0235.2015.09.154 (in Chinese).
He, T.H., Lu, S.F., Li, W.H., et al., 2018. Effect of salinity on source rock Formation and its control on the oil content in shales in the Hetaoyuan formation from the Biyang depression, Nanxiang Basin, Central China. Energy Fuels 32, 6698–6707. https://doi.org/10.1021/acs.energyfuels.8b01075.
He, T.H., Lu, S.F., Li, W.H., et al., 2019. Geochemical characteristics and effectiveness of thick, black shales in southwestern depression, Tarim Basin. J. Petrol. Sci. Eng. 185, 106607. https://doi.org/10.1016/j.petrol.2019.106607.
He, T.H., Lu, S.F., Li, W.H., et al., 2020. Paleoweathering, hydrothermal activity and organic matter enrichment during the formation of earliest Cambrian black strata in the northwest Tarim Basin, China. J. Petrol. Sci. Eng. 189, 106987. https://doi.org/10.1016/j.petrol.2020.106987.
Hu, G.Y., Li, J., Li, J., et al., 2010. The origin of natural gas and the hydrocarbon charging history of the Yulin gas field in the Ordos Basin, China. Int. J. Coal Geol. 81 (4), 381–391. https://doi.org/10.1016/j.coal.2009.07.016.
Hu, P.A., Li, J., Zhang, W.Z., et al., 2007. Geochemical characteristics and genetic types of natural gas from upper, lower Paleozoic and Mesozoic in Ordos Basin. Science in China D: Earth Sci. 37 (z2), 157–166 (in Chinese).
Hou, F.H., Fang, S.X., Dong, Z.X., et al., 2003. The developmental characters of sedimentary environments and lithofacies of middle Ordovician Majiagou formation in Ordos Basin. Acta Sedimentol. Sin. 21 (1), 106–112. https://doi.org/10.3969/j.issn.1000-0550.2003.01.016 (in Chinese).
Huang, H., 2015. The Rock Physics Experimental Study of CBM Reservoir. Chengdu University of Technology (in Chinese).
Huang, S.P., Duan, S.F., Wang, Z.C., et al., 2019. Affecting factors and application of the stable hydrogen isotopes of alkane gases. Petrol. Explor. Dev. 46 (3), 518–530. https://doi.org/10.1016/S1876-3804(19)60032-7.
Kong, Q.F., Zhang, W.Z., Li, J.F., et al., 2019. Geochemical characteristics and genesis of Ordovician natural gas under gypsolyte in Ordos Basin. Nat. Gas Geosci. 30 (3), 423–432. https://doi.org/10.11764/j.issn.1672-1926.2018.12.020 (in Chinese).
Landais, P., Michels, R., Elie, M., 1994. Are time and temperature the only constraints to the simulation of organic matter maturation. Org. Geochem. 22 (3–5), 617–630. https://doi.org/10.1016/0146-6380(94)90128-7.
Li, W., Tu, J.Q., Zhang, J., et al., 2017. Accumulation and potential analysis of self-sourced natural gas in the Ordovician Majiagou formation of Ordos Basin, NW China. Petrol. Explor. Dev. 44 (4), 521–530. https://doi.org/10.1016/S1876-3804(17)30064-2.
Li, X.Q., Hu, G.Y., Li, J., et al., 2008. The characteristics and sources of natural gases from Ordovician weathered crust reservoirs in the Central Gas Field in the Ordos Basin. Chin. J. Geochem. 27 (2), 109–120. https://doi.org/10.1007/s11631-008-0109-z.
Li, J., Li, J., Li, Z.S., et al., 2018. Characteristics and genetic types of the lower Paleozoic natural gas, Ordos Basin. Mar. Petrol. Geol. 89 (1), 106–119. https://doi.org/10.1016/j.marpetgeo.2017.06.046.
Li, J.J., 2008. Kinetic Study of Hydrogen Isotopic Fractionation during the Generation of Natural Gas and its Application. Daqing Petroleum Institute.
Li, W.H., Zhang, Q., Chen, Q., et al., 2020. Sedimentary evolution of early Paleozoic in Ordos Basin and its adjacent areas. J. NW Univ. 50 (3), 456–479. https://doi.org/10.16152/j.cnki.xdxbzr.2020-03-016 (in Chinese).
Li, X.Q., Xiao, X.M., Mi, J.K., et al., 2005. Kinetic Parameters of methane generated from source rocks and its application in the Kuqa depression of the Tarim Basin. Acta Geol. Sin. 79 (1), 134–143. https://doi.org/10.3321/j.issn:0001-5717.2005.01.015 (in Chinese).
Li, W.B., Lu, S.F., Li, J.Q., et al., 2020. Carbon isotope fractionation during shale gas transport: mechanism, characterization and significance. Science in China D: Earth Sci. 63 (5), 674–689. https://doi.org/10.1007/s11430-019-9553-5.
Liu, D., Zhang, W.Z., Kong, Q.F., et al., 2016. Lower Paleozoic source rocks and natural gas origins in Ordos Basin, NW China. Petrol. Explor. Dev. 43 (4), 591–601. https://doi.org/10.1016/S1876-3804(16)30069-6.
Liu, J.L., Liu, K.Y., Liu, C., 2019. Quantitative evaluation of gas generation from the Upper Paleozoic coal, mudstone and limestone source rocks in the Ordos Basin, China. J. Asian Earth Sci. 178, 224–241. https://doi.org/10.1016/j.jseaes.2018.04.001.
Liu, D.H., Zhang, H.Z., Dai, J.X., et al., 2000. Experimental study and evaluation on hydrocarbon generation of macerals. Chin. Sci. Bull. 45 (14), 1270–1276.
Liu, X.S., Xi, S.L., Fu, J.H., et al., 2000. Natural gas generation in the upper Paleozoic in the Ordos Basin. Nat. Gas. Ind. 20 (6), 19–23. https://doi.org/10.3321/j.issn:1000-0976.2000.06.005 (in Chinese).
Liu, R.H., Li, J., Xiao, Z.Y., et al., 2019. Geochemical characteristics and their gas and oil source correlation implication in the Tugeerming area of the Kuqa Depression, Tarim Basin, China. J. Nat. Gas Geosci. 4 (3), 161–168. https://doi.org/10.1016/j.jnggs.2019.06.001.
Lorant, F., Prinzhofer, A., Behar, F., et al., 1998. Carbon isotopic and molecular constraints on the formation and the expulsion of thermogenic hydrocarbon gases. Chem. Geol. 147 (3–4), 249–264. https://doi.org/10.1016/S0009-2541(98)00017-5.
Lorant, F., Behar, F., Vandenbroucke, M., 2000. Methane generation from methylated aromatics:Kinetic study and carbon isotope modeling. Energy Fuels 14, 1143–1155. https://doi.org/10.1021/ef990258e.
Lu, S.F., Liu, X.Y., Qu, J.Y., et al., 1995. Restoring of original hydrocarbon potential and original organic carbon of source rocks in huhehu depression Hailar Basin. J. Daqing Pet. Inst. 19 (1), 31–34 (in Chinese).
Lu, S.F., Xue, H.T., Zhong, N.N., 2003. Simulating calculation of the variations of organic matter abundance and hydrocarbon-generation Potential during geological processes. Geol. Rev. 49 (3), 292–297. https://doi.org/10.3321/j.issn:0371-5736.2003.03.011 (in Chinese).
Lu, S.F., Li, J.J., Xue, H.T., et al., 2019. Pyrolytic gaseous hydrocarbon generation and the kinetics of carbon isotope fractionation in representative model compounds with different chemical structures. G-cubed 20, 1773–1793. https://doi.org/10.1029/2018GC007722.
Ma, C.S., Xu, H.Z., Gong, C.H., et al., 2011. Paleo oil reservoir and Jingbian natural gas field of Ordovician weathering crust in Ordos Basin. Nat. Gas Geosci. 22 (2), 280–286 (in Chinese).
Mi, J.K., Wang, X.M., Zhu, G.Y., et al., 2012. Origin determination of gas from Jingbian gas field in Ordos basin collective through the geochemistry of gas from inclusions and source rock pyrolysis. Acta Petrol. Sin. 28 (3), 859–869 (in Chinese).
Meng, Z.P., Liu, C.Q., He, X.H., et al., 2008. Experimental research on acoustic wave velocity of coal measures rocks and its influencing factors. J. Min. Saf. Eng. 25 (4), 389–393. https://doi.org/10.3969/j.issn.1673-3363.2008.04.003 (in Chinese).
Ni, Y.Y., Liao, F.R., Gong, D.Y., et al., 2019. Stable carbon and hydrogen isotopic characteristics of natural gas from Taibei sag, Turpan-Hami Basin, NW China. Petrol. Explor. Dev. 46 (3), 531–542. https://doi.org/10.1016/S1876-3804(19)60033-9.
Rooney, M.A., Claypool, G.E., Chung, H.M., 1995. Modeling thermogenic gas generaion using carbon isotope ratios of natural gas hydrocarbons. Chem. Geol. 126 (3), 219–232. https://doi.org/10.1016/0009-2541(95)00119-0.
Schenk, H.J., Di Primio, R., Horsfield, B., 1997. The conversion of oil into gas in petroleum reservoirs. Part 1: comparative kinetic investigation of gas generation from crude oils of lacustrine, marine and fluviodeltaic origin by programmed-temperature closed-system pyrolysis. Org. Geochem. 26 (7), 467–481. https://doi.org/10.1016/S0146-6380(97)00024-7.
Schoell, M., 1980. The hydrogen and carbon isotopic composition of methane from natural gases of various origins. Geochem. Cosmochim. Acta 44 (5), 649–661. https://doi.org/10.1016/0016-7037(80)90155-6.
Schoell, M., 1983. Genetic characterization of natural gases. AAPG (Am. Assoc. Pet. Geol.) Bull. 67 (12), 2225–2238. https://doi.org/10.1306/AD46094A-16F7-11D7-8645000102C1865D.
Stahl, W.J., 1977. Carbon and nitrogen isotopes in hydrocarbon research and exploration. Chem. Geol. 20, 121–149. https://doi.org/10.1016/0009-2541(77)90041-9.
Sweeney, J.J., Burnham, A.K., 1990. Evaluation of a simple model of vitrinite reflectance based on chemical kinetics. AAPG Bull. 74 (10), 1559–1570. https://doi.org/10.1306/0C9B251F-1710-11D7-8645000102C1865D.
Sun, X.G., Qin, S.F., Luo, J., et al., 2001. A study of activation energy of coal macerals. Geochimica 30 (6), 599–604. https://doi.org/10.3321/j.issn:0379-1726.2001.06.013 (in Chinese).
Shi, J.A., Shao, Y., Zhang, S.C., et al., 2009. Lithofacies Paleogeography and sedimentary environment in Ordovician Majiagou formation, Eastern Ordos Basin. Nat. Gas Geosci. 20 (3), 316–324 (in Chinese).
Shuai, Y.H., Zou, Y.R., Peng, P.A., 2003a. Kinetic model for the stable carbon isotope of methane:the state of the art. Adv. Earth Sci. 18 (3), 405–411. https://doi.org/10.3321/j.issn:1001-8166.2003.03.013 (in Chinese).
Shuai, Y.H., Zou, Y.R., Peng, P.A., 2003b. Kinetics modeling of stable carbon isotopes of coal-generated methane and its significance for gases accumulation in the Kuqa Depression. Tarim Basin. Geochimica. 32 (5), 469–475. https://doi.org/10.3321/j.issn:0379-1726.2003.05.008 (in Chinese).
Tu, J.Q., Dong, Y.G., Zhang, B., et al., 2016. Discovery of effective scale source rocks of the Ordovician Majiagou Fm in the Ordos Basin and its geological significance. Nat. Gas. Ind. 36 (5), 15–24. https://doi.org/10.3787/j.issn.1000-0976.2016.05.002.
Wang, B., 2010. Evaluating the Gas Filling Capability of Shanxi Formation in Sulige Area of Ordos Basin. Chengdu University of Technology (in Chinese).
Wang, S., Wang, Y.F., Zhang, J., 2019. Geochemical characteristics of hydrocarbon source rocks of the upper Paleozoic in Eastern Ordos Basin. Liaoning Chem. Ind. 48 (8), 836–837. https://doi.org/10.3969/j.issn.1004-0935.2019.08.038 (in Chinese).
Wang, Y.N., Ren, J.F., Yang, W.J., et al., 2015. Gas accumulation characteristics and Potential of Ordovician Majiagou reservoirs in the center-East of Ordos Basin.

Mar. Orig. Petrol. Geol. (4), 33–41. https://doi.org/10.3969/j.issn.1672-9854.2015.04.004 (in Chinese).
Wang, X.F., Liu, W.H., Xiu, Y.C., et al., 2012. Effect of water medium on hydrogen isotope composition of gaseous hydrocarbon formation and evolution. Science in China D: Earth Sci. 42 (1), 103–110 (in Chinese).
Xu, S.F., 2008. Study on Drilling Formation Engineering Characteristic Based on Rock Physical Property. China University of petroleum. https://doi.org/10.7666/d.y1362649 (in Chinese).
Xie, J.L., Wu, X.Y., Sun, L.Y., et al., 2013. Lithofacies palaeogeography and Potential zone prediction of Ordovician Majiagou Member-5 in Ordos Basin. Mar. Orig. Petrol. Geol. 18 (4), 23–32. https://doi.org/10.3969/j.issn.1672-9854.2013.04.004 (in Chinese).
Xia, X.Y., 2002. Rules of petroleum source correlation and their application in the Changqing gas field-a reply to "Feature of mixed gas in central gas field of Ordos basin.". Petrol. Explor. Dev. 29 (5), 101–105. https://doi.org/10.3321/j.issn:1000-0747.2002.05.034 (in Chinese).
Xiong, Y.Q., Geng, A.S., Liu, J.Z., et al., 2004. Kinetic-simulating experiment combined with GC-IRMS analysis: application to identification and assessment of coal-derived methane from Zhongba Gas Field (Sichuan Basin, China). Chem. Geol. 213 (4), 325–338. https://doi.org/10.1016/j.chemgeo.2004.07.007.
Yang, H., Zhang, W.Z., Zan, C.L., et al., 2009. Geochemical characteristics of Ordovician subsalt gas reservoir and their significance for reunderstanding the gas source of Jingbian Gasfield, East Ordos Basin. Nat. Gas Geosci. 20 (1), 8–14 (in Chinese).
Yang, H., Fu, J.H., Wei, X.S., et al., 2011. Natural gas exploration domains in Ordovician marine carbonates, Ordos Basin. Acta Pet. Sin. 32 (5), 733–740 (in Chinese).
Yang, H., Bao, H.P., Ma, Z.R., 2014. Reservoir-forming by lateral supply of hydrocarbon:A new understanding of the formation of Ordovician gas reservoirs under gypsolyte in the Ordos Basin. Nat. Gas. Ind. 34 (4), 19–26. https://doi.org/10.3787/j.issn.1000-0976.2014.04.003 (in Chinese).
Yang, J.H., Hang, B.J., 2019. Origin and migration model of natural gas in L gas field, eastern slope of Yinggehai Sag, China. Petrol. Explor. Dev. 46 (3), 471–481. https://doi.org/10.1016/S1876-3804(19)60028-5.
Yao, J.L., Wang, C.C., Chen, J.P., et al., 2016. Distribution characteristics of subsalt carbonate source rocks in Majiagou Formation,Ordos Basin. Nat. Gas Geosci. 27 (12), 2115–2126. https://doi.org/10.11764/j.issn.1672-1926.2016.12.2115 (in Chinese).
Yu, Z., Ding, Z.C., Wu, D.X., et al., 2017. Sedimentary facies evolution model of Ordovician Majiagou formation,Central-Eastern Ordos Basin. Mar. Petrol. Geol. 22 (3), 12–22. https://doi.org/10.3969/j.issn.1672-9854.2017.03.002 (in Chinese).
Yu, C., Huang, S.P., Gong, D.Y., et al., 2013. Partial reversal cause of carbon and hydrogen isotope compositions of natural gas:a case study in Sulige gas field, Ordos Basin. Acta Petrol. Sin. 34 (S1), 92–101. https://doi.org/10.7623/syxb2013S1011 (in Chinese).
Zhang, H.Z., 2005. Kinetic Simulation of Thermogenic Natural Gas Generation and its Geological Applications. Guangzhou Institute of Geochemistry, Chinese Academy of Sciences (in Chinese).
Zhao, J.Z., Wang, D.X., Sun, L.Y., et al., 2015. Origin of the Ordovician gas and its accumulation patterns in Northwestern Ordos Basin. Oil Gas Geol. 36 (5), 711–720. https://doi.org/10.11743/ogg20150501 (in Chinese).
Zhu, J.H., Lv, J.H., Liao, J.J., et al., 2011. Hydrocarbon generation potential of lower Paleozoic source rocks in southwestern margin of Ordos Basin. Petrol. Geol. Exp. 33 (6), 662–670. https://doi.org/10.3969/j.issn.1001-6112.2011.06.019 (in Chinese).
Zhou, X.Y., 2014. The Hydrocarbon-Generation Potential Evaluation in Majiagou Group of Ordos Basin. Chengdu University of Technology.